ASSIMILATION OF AVHRR, GROUND WAVE RADAR AND RADARSAT SAR DATA INTO A COASTAL CIRCULATION AND OIL SPILL MODELLING SYSTEM

Donald O. Hodgins
President, Seaconsult Marine Research Ltd.
8805 Osler Street, Vancouver, Canada V6P 4G1

Commission VII, Working Group 5

KEY WORDS: Remote sensing. Data Assimilation. Circulation Modelling. Oil spill modelling. Coastal zone protection.

ABSTRACT

Operational three-dimensional ocean circulation models have been developed for the western Canadian continental shelf and the Georgia-Fuca inland waterway. Assimilation of near real-time SST data from AVHRR imagery using a nudging scheme, and surface current measurements from SeaSonde HF radars with an error-dependent weighted blending method has led to significant improvements in surface current prediction accuracy. An oil spill trajectory and weathering model has been coupled into the circulation model, utilizing the most recent current data for the advective calculations. RADARSAT SAR image classification, combined with computerized editing tools, is used to monitor oil slicks and parameterize slick features for re-initializing the oil spill model. Model data are distributed via the Internet for assessment by users. The integrated SEACAST system provides response organizations and monitoring agencies with timely, accurate information for decision making, taking maximum advantage of near-real time data.

INTRODUCTION

Catastrophic and chronic oil spills in marine waters pose major challenges for environmental protection and management. Oil spill trajectory and fate models, coupled to coastal circulation models, are used to plan and carry out countermeasures for catastrophic spills. Similar models are also used to backtrack smaller spills to ships and offshore platforms to identify the responsible parties.

The accuracy and utility of such models is greatly improved through assimilation of remotely sensed data. An operational, integrated modelling system, SEACAST, has been implemented for the west coast of Canada to provide information for coastal protection and management, including oil spills. A three-dimensional prognostic circulation model (C3), which forms the core of this system, has been applied at two different grid scales: 5-km over the continental shelf and 1-km in the coastal sea between Vancouver Island and the mainland of Canada and the United States. An oil spill model (SPILLSIM), coupled to the circulation model, provides predictions of the dispersion, spreading and weathering of a range of crude and distilled petroleum products. AVHRR SST imagery is assimilated directly into the temperature field of the hydrodynamic model in order to improve the accuracy of the baroclinic circulation.

SeaSonde high-frequency ground wave radars are used to collect real-time surface current maps with approximately 1-km resolution over a broad expanse of sea. These data are also assimilated into the circulation model over the radar's field-of-view. The current data are obtained hourly and are available to the modelling system within about 1 h of the end of the measurement cycle. Current maps of this type increase the accuracy of the modelled surface current fields, which is particularly important in areas of complex flow and high risk of spill.

Finally, classified images from Radarsat SAR are being used to identify spill location, size and relative thickness of slicks. This information is used to re-initialize the oil spill model at the satellite image time.

The SEACAST system and the use of near-real time imagery for operational modelling in the context of managing and mitigating oil spill damage in the coastal zone is described in this paper. The discussion focuses on the relationship of the different types of remote sensed data to the model requirements and how these data are processed for assimilation into a three-dimensional modelling system. The method of distributing georeferenced SEACAST results to spill response organizations over the Internet, as well as global applications of this type of system are described.

OCEAN CIRCULATION MODEL

The circulation model is comprised of a three-dimensional hydrodynamic model based on integrated forms of the Reynolds equations for turbulent flow and a fully coupled transport-diffusion model based on conservation equations for heat, salt and suspended solids. The layer-integrated forms of the Reynolds equations have been derived for two conditions: a surface layer defined by the conventional free-surface kinematic boundary condition, superimposed upon a set of fixed layers where the interfaces between layers are located at specified depths below mean sea level. In the coastal model, the surface layer thickness (typically 5 m) is sufficient to contain the tidal variation in water level. The governing hydrodynamic and transport-diffusion equations have the form shown in equations (1) to (6), written in tensor notation (Hodgins, 1976; Stronach et al., 1993).

In these equations the dependent variables are: u_i = horizontal velocity for i=1,2, vertical velocity for i=3, ρ = density, θ = dissolved or suspended substance, P_i = mean hydrostatic pressure gradient term, h = b-a, the layer thickness at time t, $\rho<u'_iu'_j>$ = Reynolds stress tensor, and $2\epsilon_{i,j,k}\omega_j\rho u_k$ = Coriolis force. Subscripts i,j,k denote summation over indices 1,2 and 3. The layers are defined by $x_3=b(t)$ at the top of the layer and x_3 = a at the bottom of the layer; b is a function of time only for the top layer.

The turbulence closure models include a Mellor-Yamada (1982) level-2 scheme for interfacial shear stress, which incorporates a bulk Richardson number dependence, and the Smagorinsky (1963) formulation for lateral shear stress, dependent on local current shear.

(i) surface layer —

$$\partial(\rho u_i h)/\partial t + \partial(\rho u_i u_j h)/\partial x_j + \partial(\rho \langle u'_i u'_j \rangle h)/\partial x_j + P_i + (\rho \langle u'_i u'_3 \rangle|_b - \rho \langle u'_i u'_3 \rangle|_a) + 2\epsilon_{i,j,k}\omega_j \rho u_k h = 0 \quad (1)$$

$$\partial \rho h/\partial t + \partial\, \rho u_i h/\partial x_i - \rho u_3(a) = 0 \quad (2)$$

$$\partial \theta h/\partial t + \partial\, \theta u_i h/\partial x_i + h\partial \langle \theta' u'_i \rangle/\partial x_i + \langle \theta' u'_i \rangle|_b - \langle \theta' u'_i \rangle|_a - \theta u_3(a) = \text{source} + \text{sink terms} \quad (3)$$

(ii) subsurface layers —

$$\partial(\rho u_i h)/\partial t + \partial(\rho u_i u_j h)/\partial x_j + \partial(\rho \langle u'_i u'_j \rangle h)/\partial x_j + P_i + (\rho \langle u'_i u'_3 \rangle|_b - \rho \langle u'_i u'_3 \rangle|_a) + (\rho u_i u_3(b) - \rho u_i u_3(a)) + 2\,\epsilon_{i,j,k}\omega_j \rho u_k h = 0 \quad (4)$$

$$\partial \rho h/\partial t + \partial\, \rho u_i h/\partial x_i + (\rho u_3(b) - \rho u_3(a)) = 0 \quad (5)$$

$$\partial \theta h/\partial t + \partial\, \theta u_i h/\partial x_i + h\partial \langle \theta' u'_i \rangle/\partial x_i + \langle \theta' u'_i \rangle|_b - \langle \theta' u'_i \rangle|_a + (\theta u_3(b) - \theta u_3(a)) = \text{source} + \text{sink terms} \quad (6)$$

Horizontal diffusion is based on constant eddy diffusivity scaled in proportion to the grid size. The dependent variables for dissolved/suspended substances include salinity (S), temperature (T) and sediment concentration (C_s). The density ρ is determined from an equation of state.

The required boundary conditions—water levels, open-boundary velocities and water properties, river runoff, and winds—are obtained from existing observing networks or from historical fields. Wind stress $\rho \langle u'_i u'_3 \rangle|_{b(t)}$ is calculated at each time step using the 10-m local wind and the drag coefficient dependence given by Large and Pond (1981). Initial conditions for ρ are specified from climatological data. The circulation models are prognostic in all dependent variables, and are spun-up from rest (u_i=0) until transients are removed from the system and it is in dynamic balance with the applied forces. At that point the model is suitable for assimilating observed surface fields from the satellite and ground wave radar sensors.

The governing equations are solved using semi-implicit finite difference methods on uniformly spaced Cartesian grids (Stronach et al., 1993). The shelf grid spacing is 5 km, while the grid spacing for the Strait of Georgia is 1 km. The number of layers and the layer thickness can be varied to resolve the important oceanic and effluent dispersion processes. Between 14 and 20 layers are used in the present applications.

OIL SPILL MODEL

A generalized oil spill model (SPILLSIM) has been developed to predict the trajectory and weathering properties of a range of petroleum products using the surface currents calculated with the circulation models. The oil spill model incorporates transport and diffusion, surface spreading, evaporation, vertical dispersion and emulsification using the Mackay et al. (1980) analytical approach. Mackay's approach treats the oil in two components, a "thick" portion of the slick and a "thin" portion. The spill is divided into a time-series of discrete parcels. Each parcel is initialized with a volume and area associated with the thick and thin slick fractions; the change in the volume and area of the slick fractions with time is then calculated as a function of the weathering processes.

Horizontal dispersion of the oil is simulated by dividing each parcel into several thousand particles. The oil volume associated with the parcel at any time is divided equally amongst the particles in order to account for weathering, shoreline, recovery and other boundary volume losses. The particles are advected by the current u_i, and diffused using a random walk model. Mathematically, each particle of oil is defined by a position vector $\mathbf{R}(t)$ with location at time t given by:

$$R(t) = \int_0^t (u_i(x_i,t) + u_i')\, dt \quad (7)$$

where $u_i(x_i,t)$ is the total surface current vector derived from the circulation models. Diffusion is produced by the turbulent part of the flow field u_i' arising from subgrid scale motions. This integral is solved in a sequence of N discrete time steps with increment Δt, for M particles comprising each oil parcel. The result is M position vectors

$$R_l(N\Delta t) = \sum_{n=1}^{N} (u_i(x_i,n\Delta t)\Delta t + s_n \times r_n); \quad l=1,2,\ldots,M \quad (8)$$

For a particle that moves a distance which is uniformly distributed in the range (0,s) in a time step Δt, the probability of the particle being at location s at time t satisfies the diffusion equation with apparent diffusivity D. The random walk step size is given by $s=(6D\Delta t)^{1/2}$. This procedure constitutes a Monte Carlo method (Bauer, 1958) where the diffusive effects of u_i' are simulated by a random walk analogy consisting of M trials each with N random displacements having magnitudes between -s and s. r_n is a random number in the range (-1,1).

Details of the weathering calculations are given in Hodgins et al. (1991) and the reference cited previously. In addition to weathering, oil absorption by the shoreline is modelled up to a limit based on substrate and the incident wave energy.

The outcome of the calculation is a set of particle positions $\mathbf{R}_l$ for each parcel comprising the spill, with attributes giving the

weathered and absorbed amounts and the oil age. The oil slick at time t is defined by the volume distribution mapped onto a Cartesian grid of points for all parcels. The oil volume in the cells of the grid are found by summing the particles for all parcels. Thus, the dependent variable field of the oil spill model is a volume distribution denoted by $V(x_i,t)$, with associated attributes.

DATA ASSIMILATION

Satellite image data are assimilated into the model as a redundant boundary condition at the sea surface. The following parameters and their data sources are presently used in the model:

Sensor	Parameter	Dependent Variable
AVHRR	SST	$T(x_i,t)$
SeaSonde HF radar	surface current	$u_i(x_i,t)$, i=1,2
SAR	surface slicks	$V(x_i,t)$

Surface Layer Temperature

The ascending NOAA-14 AVHRR "quicklook" reference images are screened daily for cloud-free conditions exceeding about 40% of the model domain and, for those images meeting this criterion, the level 1b data file is downloaded to a workstation via a DirecPC satellite data link. These image data are then navigated and processed to a set of single-band radiance image files mapped onto a georeferenced conic projection. A cloud mask is generated for the image by flagging all pixels which meet either low-temperature or high-brightness criteria, and a land mask is created by binarizing the optical-NIR (near-infrared) difference image at a suitable threshold level. The navigated radiance images are used to compute sea-surface temperature fields starting with the McLain et al. (1985) MCSST algorithm, incorporating Kidwell's (1995) correction for the satellite zenith angle, with NOAA's standard coefficients. The MCSST algorithm provides an estimate of the skin temperature of the ocean; the bulk temperature for the upper layer of the model is calculated using the regression equation:

$$T_{bulk} = 0.816\ MCSST + 2.419\ ^\circ C \qquad (9)$$

based on 175 observations from ocean buoys in the model domain.

These fields have a resolution of approximately 1.1 km and are generally spatially intermittent. They are resampled to the model grid (5 km on the shelf and 1 km in the strait) and filtered to remove unrealistic values close to land and cloud edges. The resampled field provides the calibrated $T(x_i,t)$ for assimilation. A computationally efficient nudging scheme (Ghil and Malanotte-Rizzole, 1991) is used to assimilate the surface layer field. This nudging scheme is based on a Gaussian weighting function raised to a power, centered at the image time with a period of ± 3 h. The function has a value of 1 at the image time, resulting in replacement of the modelled value with the image value. When the power applied to the function is increased, the time over which the image data modifies the modelled field is reduced; a power of 5 was found to give reasonable results over the continental shelf.

Surface Current

The SeaSonde is a compact ground wave radar system for mapping surface currents based on a frequency-modulated, continuous-wave (FMCW) signal format (Hodgins, 1995). Transmit frequencies of 12.5 and 25 MHz are typically used in coastal applications. At 12.5 MHz, the SeaSonde has a range resolution of 2.556 km over 31 range cells, giving a theoretical range of 79.2 km. The system utilizes two or more radar sites each separated by 25 to 35 km along the coast. A radar site consists of the transmit/receive hardware, a data acquisition computer, compact cross-stick or air-loop receive antennas and a monopole transmit antenna. One radar site provides a measurement of the radial velocity field within the radar's field-of-view. The radial current components $v_j(\phi_j)$ around each range ring are derived from the Doppler shift of the Bragg peaks in the sea echo spectra. Directions ϕ_j associated with each radial current are found using a least squares direction finding algorithm (Lipa and Barrick, 1983). Typically, 15 Doppler spectra are averaged to provide one hourly estimate of $v_j(\phi_j)$ and the standard deviation δv of the speed. The azimuthal resolution of the radial currents is 5°. Barrick *et al.* (1974) have shown that the current sensed by the radar backscatter represents an average over a depth proportional to the radar wavelength. This depth is approximately 0.95 m for a carrier frequency of 12.5 MHz; thus, HF radars measure a near-surface current that is a reasonable approximation for the upper layer current in the circulation model.

The radial current maps from two or more sites are then used to calculate the total current field $u_i(x_i,t)$ by combining radial currents on the uniformly spaced Cartesian model grid. A circular cell is defined around each grid point encompassing one or more radial components from each radar site. The radial velocity at the grid point is calculated as a weighted average of the radial components for one site contained in the circle. The weights incorporate the distance (weighted inversely) from the grid point to a contributing radial, and the standard deviation δv for each $v_j(\phi_j)$. Radial components from each site are combined by vector addition to give the total current magnitude and direction, and estimates of the error in speed (δr) and direction ($\delta\theta$). The current errors are spatially dependent. Confidence in the observed current, as reflected by δr and $\delta\theta$, is highest near the centre of the coverage area between the radars, where radar performance is best, and lowest toward the edges of the coverage area. The larger separation between radial currents with increasing range, combined with poorer radar performance at large range, and increased triangulation error in the vector addition (Leise, 1984), accounts for the lower confidence around the limits of coverage. These characteristics lead to surface current measurements that are slightly noisier than one expects from conventional current meter data. In order to take these error characteristics in account, the data assimilation scheme adopted for $u_i(x_i,t)$ blends the observed field with the modelled field at centre time of the measurement using a spatially-dependent weighting function of the form:

$$u_i(x_i,t)_A = \kappa\, u_i(x_i,t)_O + (1-\kappa)\, u_i(x_i,t)_M \qquad (10)$$

where κ is a weight, and subscripts A, O and M represent Assimilated, Observed and Modelled currents. A variable ε is defined as the ratio of the area of the tip of the current vector that is allowed to vary with $r \pm \delta r$ and $\theta \pm \delta\theta$ to the area of the annular ring segment defined by $r \pm \delta r_{max}$ and $\theta \pm \delta\theta_{max}$. The weight κ is defined as $0.75(1-\varepsilon)$. The factor

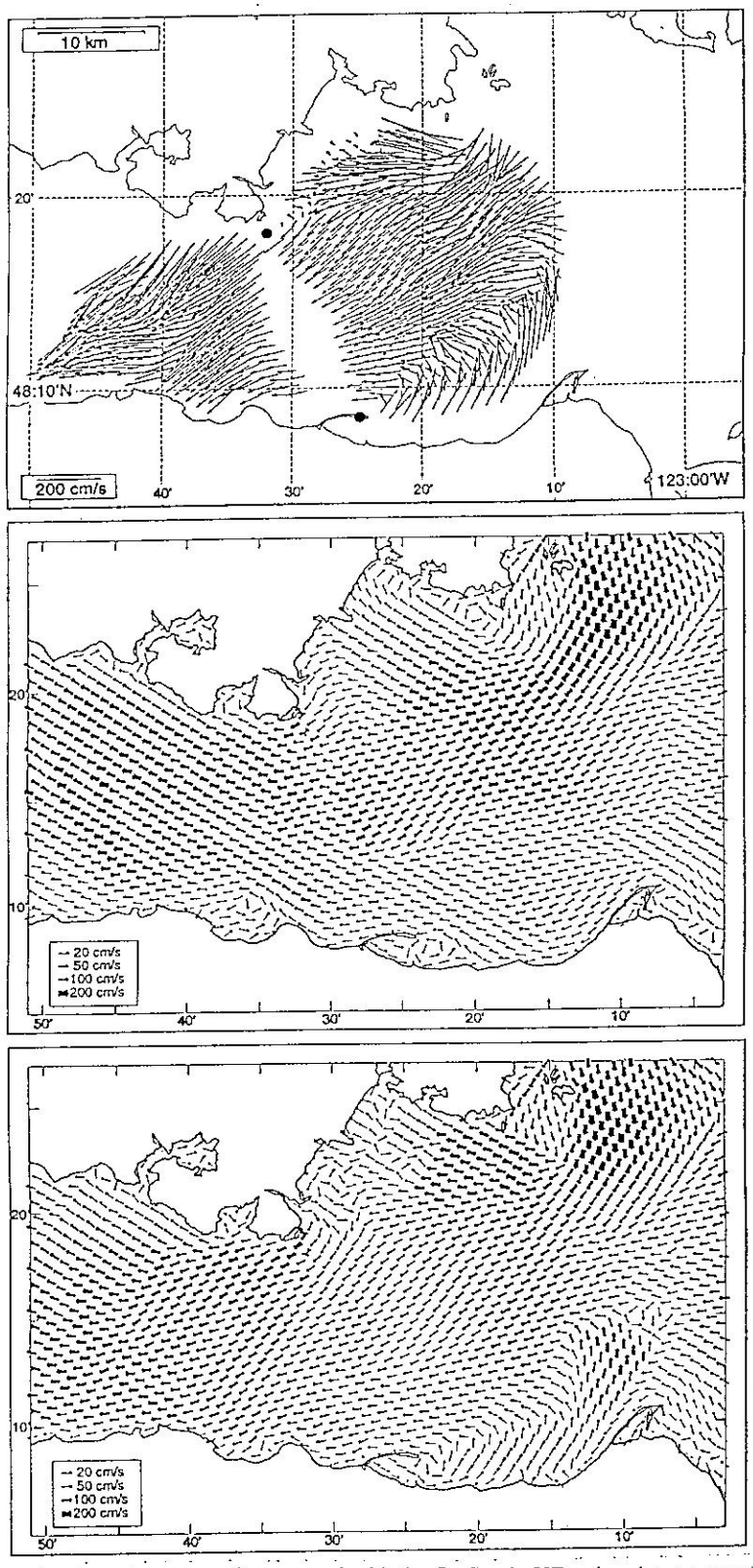

Figure 1 Ebb surface current pattern (upper panel) measured with the SeaSonde HF radar, (centre panel) modelled and (lower panel) modelled with data assimilation.

0.75 ensures that the modelled field in (10) always exerts some influence on the final estimate at each grid point; since the modelled fields are spatially smoother than the SeaSonde measurements, this weight provides some smoothing of noise the assimilated field. The observed currents are assimilated into the circulation model by applying equation (10) to each hourly measurement, without time nudging.

Figure 1 illustrates a typical ebb tide surface current field in Juan de Fuca Strait, British Columbia. The measured field using two SeaSonde radars on opposite sides of the strait is shown in the upper panel. The modelled field, without assimilation, is shown in the centre panel, and the blended field is shown in the lowest panel. The average κ-field for 3 weeks of hourly assimilations is shown in Figure 2 and illustrates the expected decrease in κ towards the edges of the coverage area and along the baseline zone where surface currents cannot be estimated from the radial components.

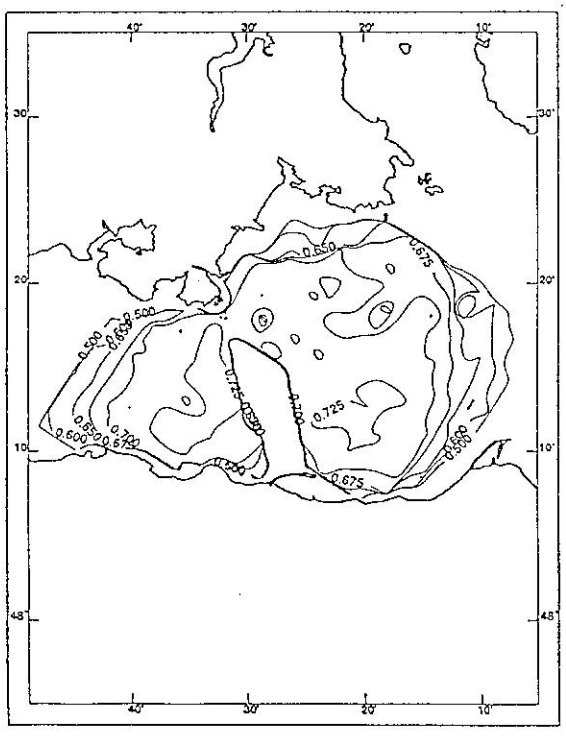

Figure 2 Spatial Distribution of the Mean Weight κ for 500 SeaSonde Current Assimilations.

Oil Slicks

Previous studies using ERS-1 synthetic aperture radar (SAR) indicated that hydrocarbon oil slicks could be detected in the imagery under suitable low-wind conditions (Bern et al., 1992). Using recent RADARSAT SAR images of the *Sea Empress* oil spill at Milford Haven in 1996 and the *Nakhodka* fuel oil spill in the Sea of Japan in January 1997, Hodgins et al. (1997a, 1997b) have shown that it is possible to monitor oil distributions on the sea and classify the images for areas that are heavily oiled, areas that are lightly oiled and areas that are free of oil. A composite 3-scene SAR image obtained on January 11, 1997, for the *Nakhodka* spill in the Sea of Japan is shown in Figure 3. The main source of the spilled fuel oil was from the grounded bow section of the tanker approximately 200 m offshore of Mikuni. This image suggests that the heavy oil patch originating at Mikuni is surrounded by a transition zone of lighter oiling, consistent with the application of dispersants used by the response agencies. It also displays low-brightness areas associated with unstable atmospheric conditions behind a front passing over the area.

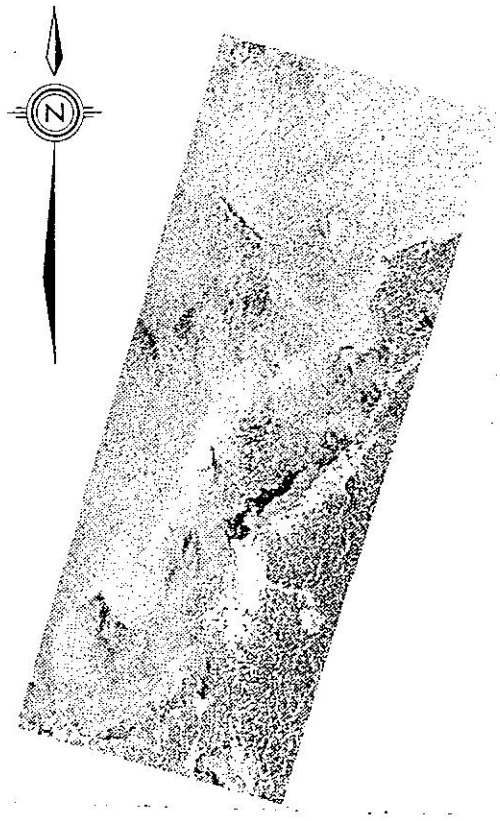

Figure 3 Composite SAR Image of the *Nakhodka* spill, Jan. 11, 1997.

Image classification involves speckle reduction using a 15x15 Lee adaptive filter, followed by calculation of frequency distributions of reflectance from selected training areas spanning heavy oil to background sea and selection of thresholds to delineate areas with differing oil coverage. Applying three thresholds to the digital values (DV) over the entire SAR scene image yields a classified image as shown in Fig. 4. Matching the thresholds with categories in Environment Canada's oil observing scheme provides a relative scaling to oil thickness (Table 1).

The classified images contain the slick features, but also false features that are atmospheric in origin. Moreover, the area associated with each slick class will be sensitive to the thresholds set for the class. In order to provide for human judgment in the assimilation process, an interactive scheme allowing the SEACAST modeller to view the SAR image, the classified SAR image and the oil distribution predicted by the model within the oil spill model's geographic canvas has been developed. The software also provides a graphical editor to map and re-classify the delineated slicks as a set of polygons linked to oil classes (Fingas et al., 1979). Once the polygon set has been derived, the volume of oil on the water $V(x_i,t)$ is mapped into the polygons weighting the volumes by the relative thickness of the classes. The final result is a new allocation of volume matched to the polygon locations. This reinitializing editor provides the man-machine link between SPILLSIM and either the enhanced SAR image, or the classified SAR image, both of which are viewed as data layers through the interface.

Table 1: Classification Thresholds and Relationship to Visible Oil Groups

DV SEACAST Threshold	Hypothetical Image Colour	Thickness (μm)	Oil Appearance
> 7700	light grey	0.0	Ambient sea
3000 < DV ≤ 7700	mid-grey	0.08	Visible as silvery sheen (light oiling)
≤ 3000	dark grey	2.0	Darker brown colours (heavy oiling)

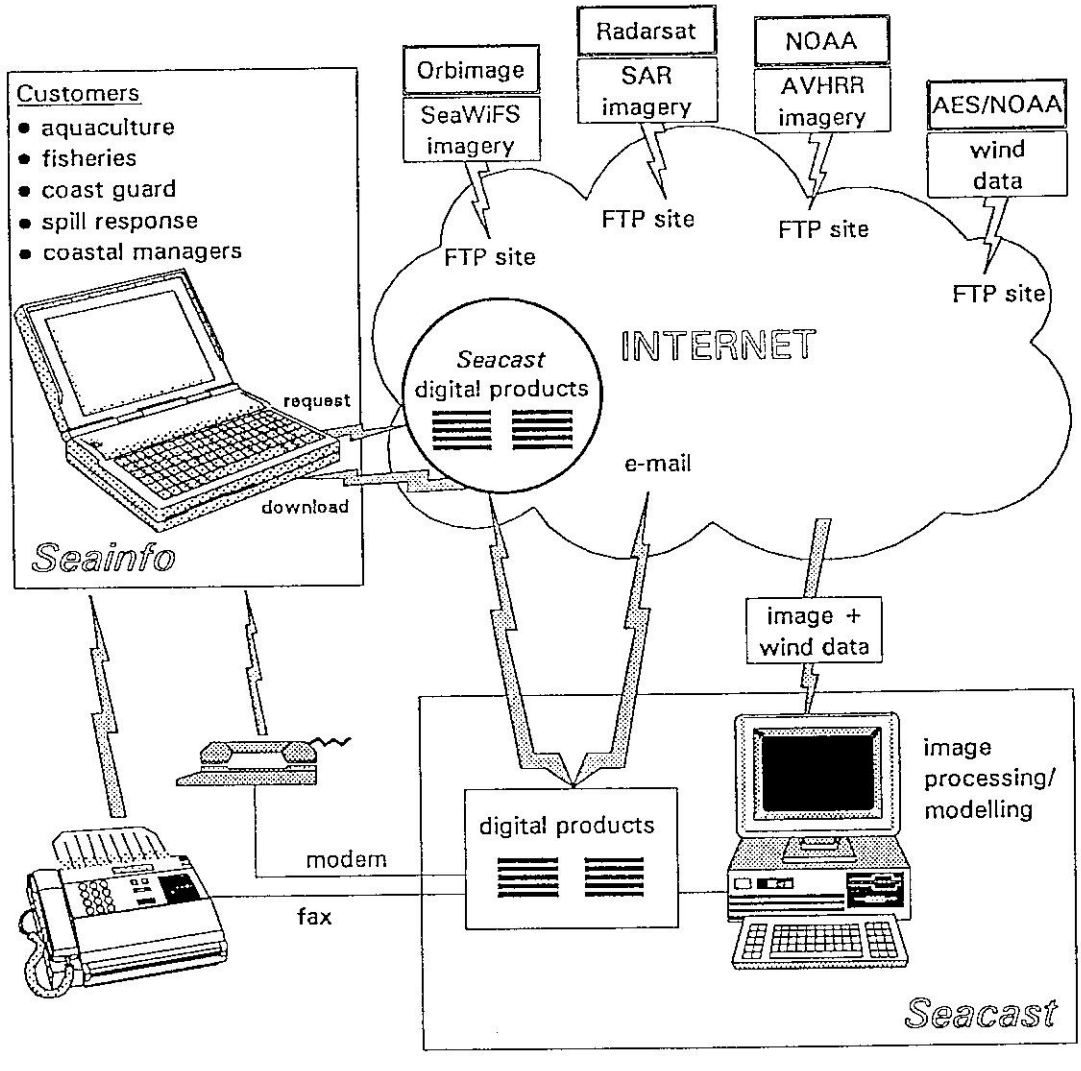

Figure 5 Data Flow Diagram for the SEACAST System Showing Data Dissemination Over the Internet.

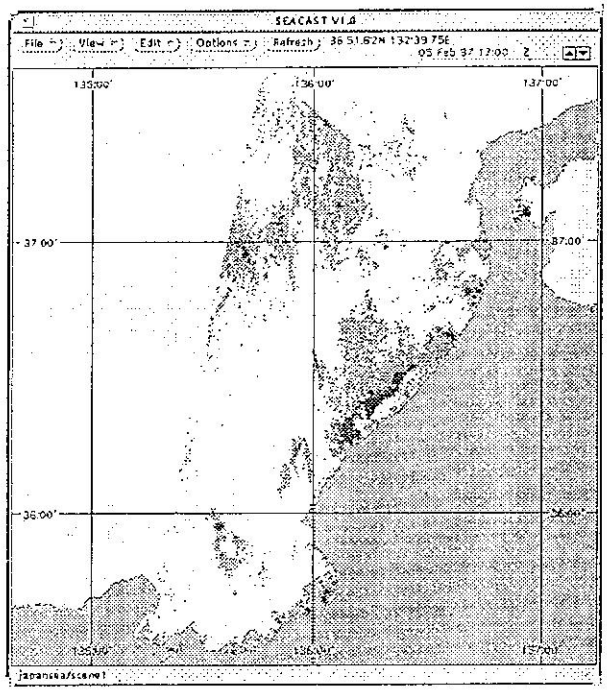

Figure 4 Classified Image of the SAR Image in Figure 3.

DATA DISSEMINATION

The SEACAST circulation models are run daily reinitializing all dependent variable fields using results at -120 hours (5 days old). The models are then run forward in time assimilating all available SST image data and a 48-hour forecast is generated. When the SeaSonde is on-line, these data are assimilated hourly. During an oil spill, the spill model is run as frequently as updates are required by the response organizations drawing current and wind input data from the circulation models. Generally, updates are required every few hours during the first day or two of an emergency, and then less frequently as the response becomes organized. When RADARSAT SAR images are obtained, they are used to monitor the spill and reinitialize the spill model.

The output from the system consists of fields from the hydrodynamic model—SST, salinity, surface current—and oil slick information—volume distributions, oil volume balance, oil properties—from the spill model. These fields are generated at the frequency required by the user, and in the case of the spill model this is typically every 20-30 minutes. All fields derived from SEACAST are uniformly stored in georeferenced, binary format and distributed to users over the Internet. The data flow for SEACAST is illustrated in Figure 5. The digital output files are placed in password-protected web pages and can be accessed by all entitled users at their convenience. A data-viewing Windows program (*Seainfo*) is provided to users, allowing them to display and manipulate the model output. This system provides response organizations and agencies responsible for monitoring oil spill response with timely, accurate information for decision making, taking maximum advantage of near-real time data.

An example of the *Nakhodka* spill model file after re-initialization presented in *Seainfo* is shown in Figure 6.

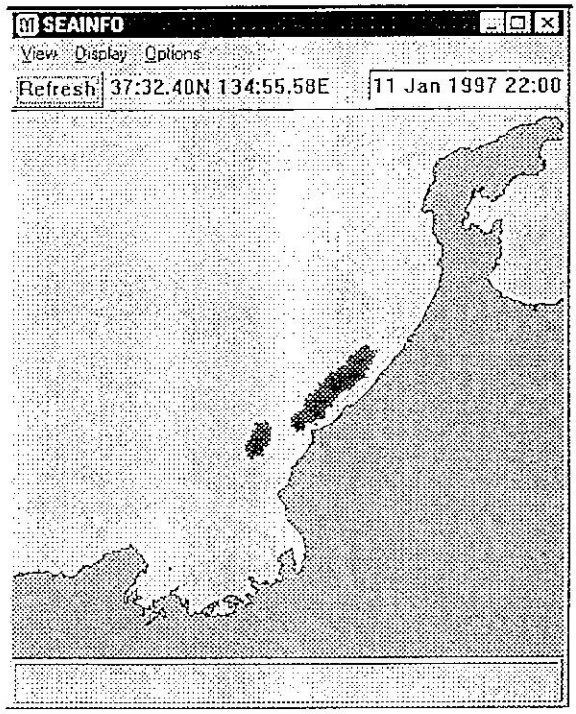

Figure 6 SPILLSIM Slick Prediction Based on SAR Image Re-initialization (*Nakhodka* Spill, Sea of Japan).

CONCLUSIONS

Three-dimensional circulation models have been implemented and verified for the Canadian west coast at two scales of resolution: a 5-km continental shelf model and a 1-km model for the Georgia-Fuca waterway which is a large coastal sea connected to the Pacific Ocean. Methods to successfully assimilate near real-time sea surface temperature data from AVHRR imagery and surface current measurements from ground wave radars into these circulation models have been developed and tested. Data nudging using a Gaussian distribution in time with a 6-hour window was found to be the most appropriate method for SST. A data blending scheme based on weights derived from the error characteristics of the ground wave radar (SeaSonde) systems, without time-dependent nudging, appears optimum for current assimilation. Assimilation of these data provides significant improvements in surface current prediction accuracy from the models. An oil spill trajectory and weathering model has been coupled into the circulation model, utilizing the most recent current data for the advective calculations. Classification techniques for RADARSAT SAR imagery, combined with computerized graphical editing tools, has led to practical methods for monitoring oil slicks and parameterizing the observed slick features into re-initialization fields for the oil spill model. The circulation modelling system runs operationally on a 24-h cycle on a Sun Unix workstation, computing a 5-day hindcast with data assimilation and a 2-day forecast. Oil spill simulations are computed as required for contingency planning and emergency response.

The modelling systems have global applicability. Data products, in the form of surface current, temperature and salinity fields, as well as predicted oil slick (volume) distributions can be distributed to users over the Internet and

simple, Windows data viewing programs are available to display and query results.

REFERENCES

Barrick, D.E., J.M. Headrick, R.W. Bogle and D.D. Crombie, 1974. Sea Backscatter at HF: Interpretation and Utilization of the Echo. Proc. IEEE. 62, pp 673-680.

Bauer, W.F., 1958. The Monte Carlo Method. J. Soc Indust. Appl. Math., 6(4), pp 438-451.

Bern, T.-I., S. Barstow, and S. Moen, 1992. Oil Spill Detection Using Satellite-based SAR, Report no. OCN R-92096, Prepared by Oceanor, Trondheim, Norway.

Fingas, M.F., W.S. Duval and G.B Stevenson, 1979. *The Basics of Oil Spill Cleanup*, Environment Canada, Ottawa, 155 p.

Ghil, M. and P Malanotte-Rizzole, 1991. Data assimilation in meteorology and oceanography. Adv. Geophys., 33, pp 141-266.

Hodgins, D.O., 1976. On Certain Aspects of a Numerical Model for Three-dimensional Stratified Flows. Report Series No. 14, Int. Institute of Hydraulic and Environmental Engineering, Delft.

Hodgins, D.O., 1994. Remote Sensing of Ocean Surface Currents with the SeaSonde HF Radar. Spill Science & Technol. Bull., 1(2), pp 109-129.

Hodgins, D.O. J.H. Huang, D.S. Dunbar and S.L.M. Hodgins, 1991. A High-resolution Coupled Hydrodynamic and Oil Spill Modelling System Applied to the Port of Vancouver, Proc. Arctic and Marine Oilspill Program (AMOP) Technical Seminar, June 1991, Vancouver, pp. 39-56.

Hodgins, D.O., S.S. Salvador, S.E. Tinis and D. Nazarenko, 1997a. RADARSAT SAR For Oil Spill Response. Proc. Arctic and Marine Oilspill Program (AMOP) Technical Seminar, June 1997, Vancouver, pp. 1031-1039.

Hodgins, D.O., S.S. Salvador, S.E. Tinis and D. Nazarenko, 1997b. RADARSAT SAR For Oil Spill Response. Spill Science & Technol. Bull., 3(4), pp 241-246.

Kidwell, K.B., 1995. *NOAA Polar Orbiter Data Users Guide*. Publication of the National Oceanic and Atmospheric Administration, National Environmental Satellite Data and Information Service, National Climatic Data Centre, Satellite Services Division. Washington, D.C.

Large, W.G. and S. Pond 1981. Open Ocean Momentum Flux Measurements in Moderate to Strong Winds. J. Phys. Oceanogr., 11, pp 324-336.

Leise, J.A., 1984. The Analysis and Digital Signal Processing of NOAA's Surface Current Mapping System. IEEE J. Oceanic Engrg. OE-9(2), pp 106-113.

Lipa, B.J. and D.E. Barrick 1983. Least-squares Methods for the Extraction of Surface Currents from CODAR Crossed-loop Data: Application at ARLSOE. IEEE J. Oceanic Engrg. OE-8(4), pp 226-253.

Mackay, D., S. Paterson, and K. Trudel, 1980. A Mathematical Model of Oil Spill Behaviour. Unpublished Manuscript, Dept. of Chemical Engineering, Univ. of Toronto.

McClain, E.P., W.G. Pichel, and C.C. Walton, 1985. Comparative Performance of AVHRR-Based Multichannel Sea Surface Temperatures. Journal of Geophysical Research, 90, pp 11587-11601.

Mellor, G.T. and T. Yamada, 1982. Development of a Turbulence Closure Model for Geophysical Fluid Problems. Rev. Geophysics and Space Physics, 20(4), pp 851-875.

Smagorinsky, J., 1963. General Circulation Experiments with the Primitive Equations. I. The Basic Experiment. J. Mon. Weather Rev., 91, pp 99-164.

Stronach, J.A., J.O. Backhaus and T.S. Murty, 1993. An Update on the Numerical Simulation of Oceanographic Processes in the Waters Between Vancouver Island and the Mainland: the GF8 Model. Oceanogr. Mar. Biol. Annu. Rev., 31, pp 1-86.